Journal of Civil and Hydraulic Engineering
https://www.acadlore.com/journals/JCHE

Development of an Intelligent Monitoring Framework for Concrete Tensioning Quality Based on the Radial Basis Function Neural Network

Jie Chen, Kenan Zhao, Kai Sun*

School of Civil Engineering and Transportation, North China University of Water Resources and Electric Power, 450045 Zhengzhou, China

* Correspondence: Kai Sun (sunkai@ncwu.edu.cn)

Received: 10-19-2024 **Revised:** 03-24-2025 **Accepted:** 04-25-2025

Citation: J. Chen, K. N. Zhao, and K. Sun, "Development of an intelligent monitoring framework for concrete tensioning quality based on the radial basis function neural network," *J. Civ. Hydraul. Eng.*, vol. 3, no. 2, pp. 100–112, 2025. https://doi.org/10.56578/jche030204.

Abstract: Traditional tensioning monitoring techniques for prestressed concrete structures often exhibit limitations in real-time performance, accuracy, and adaptability to complex stress distributions. To address these challenges, an intelligent monitoring framework is developed based on a Radial Basis Function (RBF) neural network. Using the Dongjiacun aqueduct as a case study, a comprehensive methodology is established, integrating numerical simulation, Machine Learning (ML), and real-time data processing. Initially, Finite Element Analysis (FEA) is conducted to simulate stress distribution during the tensioning process, allowing for the extraction of critical stress data at key structural locations. These data serve as the foundation for training the RBF neural network, which functions as a high-fidelity surrogate model capable of efficiently predicting stress variations with enhanced accuracy. By leveraging the network's strong generalization capabilities, the proposed framework ensures rapid and precise estimation of stress evolution throughout the tensioning process. Furthermore, an intelligent monitoring platform is designed, incorporating real-time data acquisition, automated stress prediction, and visualization functionalities. The platform facilitates prestress control and structural health assessment, contributing to the long-term safety and durability of prestressed concrete structures. Additionally, an interactive user interface is prototyped using Mock Plus to enhance usability and facilitate intuitive interpretation of stress-related insights. The proposed approach not only advances the automation and intelligence of tensioning monitoring but also provides a robust technical foundation for optimizing prestress management in large-scale infrastructure applications.

Keywords: Radial Basis Function (RBF); Finite Element Analysis (FEA); Surrogate model; Structural health monitoring; Mock plus

1 Introduction

In large-span structures, prestressed systems are widely used because they can counteract part of the tensile stress caused by external loads, thereby increasing the structure's load-bearing capacity and stiffness, as well as enhancing its durability and impermeability. However, during the tensioning process, due to variations in tensioning force, anchorage conditions, and construction techniques, uneven stress distribution may occur on the surface of the concrete, which affects the transmission efficiency of the prestress and the durability of the structure. To address this issue, drawing on the ideas proposed by Japanese scholars for comprehensive management of construction using computer and internet technologies, neural network technology is introduced. By combining FEA with sensor technology, this approach monitors the stress on the concrete surface, capturing real-time stress changes during construction, and providing more accurate and comprehensive stress field distribution data.

Scholars both domestically and internationally have conducted numerous studies using neural network algorithms to train surrogate models, aiming to achieve construction monitoring purposes [1]. Yamanaka et al. [2] proposed a new framework for creating surrogate models for the computational homogenization of elastoplastic composite materials, which serves as the homogenized constitutive law for decoupling two-scale analyses. Kůdela and Matoušek [3] proposed a surrogate model based on Lipschitz underestimation and used it to develop a differential evolution-based algorithm. Evangelista Junior and Almeida [4] demonstrated the generalization ability of the RBF surrogate model in predicting thousands of unseen data points from Monte Carlo simulations, successfully evaluating the uncertainty quantification of time-varying energy release rates. Antonello et al. [5] used PINN as a surrogate model for simulating accidental scenarios in nuclear power plants (NPP), showcasing PINN's advantages in providing accurate solutions, avoiding overfitting and underfitting, and inherently ensuring physically consistent results. Cao et al. [6] obtained a low failure probability by combining an iterative framework of the SS and RBF neural network surrogate models. Gholizadeh and Samavati [7] trained surrogate models using a combination of wavelet transformation, neural networks, and evolutionary algorithms to predict the dynamic response of structures, and the results indicated that the hybrid method has significant computational advantages in structural optimization dynamics design. Kazemi and Jankowski [8] improved the data-driven decision-making techniques in Python software, naming it a supervised ML algorithm, used to predict the seismic ultimate capacity of steel moment-resisting frames (MRFs) considering soil-structure interaction (SSI) effects. Goliatt et al. [9] proposed a hybrid modeling framework based on ML models (such as Extreme Learning Machine (ELM), Support Vector Regression (SVR), Extreme Gradient Boosting (XGB), and Multivariate Adaptive Regression Splines (MARS)) combined with nature-inspired differential evolution (DE) optimization for FBHP prediction. Abdedou and Soulaïmani [10] introduced the Proper Orthogonal Decomposition-Based B-Spline Bezier Element Method (POD-BSBEM) as a non-intrusive reduced-order model for uncertainty propagation analysis in stochastic time-dependent problems. Mokarram and Banan [11] proposed a new metaheuristic surrogate model called Surrogate FC-MOPSO, which significantly reduces the computational cost of solving structural multi-objective optimization problems.

In response to the complexity of finite element simulations, foreign scholars like Bagheri et al. [12] utilized surrogate-assisted optimization algorithms to find design parameter settings while minimizing the number of finite element simulations. Gribniak et al. [13] studied the effect of finite element size on the deformation prediction of reinforced concrete flexural members.

Based on finite element simulation data, using neural network algorithms to monitor the compressive strength, tensile strength, elastic modulus, and deflection of prestressed concrete structures is crucial. Numerous scholars, both domestically and internationally, have conducted research in this area. Nguyen et al. [14] introduced a novel AI-based inference model called WFR-FBI-LSSVR for the development and testing of long-term deflection prediction in reinforced concrete beams. Panda et al. [15] combined artificial neural networks (ANN) with dimensionless numerical analysis to predict the displacement response of elastically supported (ES) beams under sequential moving loads in opposite directions. Nguyen et al. [16] proposed an efficient ML model to predict the compressive and tensile strength of high-performance concrete (HPC). Dou et al. [17] introduced an inverse analysis method based on a novel hybrid firework algorithm (FWA) and RBF model to diagnose the health of concrete dams. By using displacement variations under different reservoir water levels, the elastic modulus of materials was identified to diagnose damage in concrete dams. Asteris et al. [18] emphasized that predicting the compressive strength of concrete using hybrid integrated ML techniques is a key parameter in concrete durability design and service life estimation.

The results predicted by the surrogate model can be windowed and integrated with the current stress prediction research based on RBF neural networks through digital twin (DT) technology. This integration enables real-time monitoring, model optimization, virtual simulation validation, and decision support, enhancing both the accuracy and real-time capability of stress prediction. It also provides comprehensive life-cycle management and maintenance support for prestressed structures. Wang et al. [19] proposed a DT framework for spatial structures, establishing a high-precision DT model based on offline data-driven and online data approaches. They also developed a visualization platform for cable dome structures, enabling real-time, interactive visualization. Jayasinghe et al. [20] employed ANN as a real-time alternative to finite element modeling, using sensor data and structure behavior visualization to comprehensively monitor the response of port structures.

Based on the current research, this paper proposes a tensioning quality monitoring method for concrete structures based on the RBF algorithm. Using the Dongjiacun Aqueduct as a case study, an intelligent tensioning process monitoring system was designed. Finite element simulations of the tensioning sequence for the Dongjiacun Aqueduct were conducted using ABAQUS software. The points of maximum stress, uniformly distributed stress, and stress concentration were selected as stress monitoring points, with the stress variation at these points serving as tensioning quality control indicators. The simulation data were then used as training samples to develop a surrogate model for real-time FEA of the tensioning process using the RBF neural network in Matlab. Through this surrogate model and sensor technology, the tensioning quality is monitored and controlled. If the stress at the monitoring points does not meet the required levels, additional tensioning is performed to ensure that the prestressed concrete structure achieves good tensioning quality during construction, thus ensuring the safety and reliability of the prestressed concrete structure.

2 Theory Outline

2.1 Instantaneous Prestress Loss Along the Distribution Analysis Method

Prestressed ducts are typically composed of both straight and curved sections. During the tensioning of prestressed tendons, friction arises within the duct due to factors like duct positioning errors and tendon corrosion, leading to prestress losses. In straight sections, friction occurs between the tendons and the duct walls during tensioning because of positioning errors and the roughness of the duct interior, resulting in friction losses known as deviation losses. In curved sections, the tendons exert radial pressure on the duct walls, leading to additional friction losses, referred to as curvature friction losses. Compared to straight sections, the friction losses in curved sections make up the majority of total prestress friction losses, and these losses increase significantly with larger duct curvature angles. Therefore, when calculating friction losses for straight sections, the total curvature angle from the tensioning end to the point of interest is typically assumed to be zero.

1) Friction loss $\sigma_{l1}(x)$ [21, 22]

Straight and curved prestressed steel strands:

$$\sigma_{l1} = \sigma_{con}\left[1 - e^{-(\kappa x + \mu\theta)}\right] \tag{1}$$

In the formula: σ_{con}: Tensioning control stress. θ: The sum of the curve angles of the duct from the tensioning end to the calculated section, measured in radians. k: The friction coefficient considering local deviations per meter of the duct length. Calculating straight tendons, $\theta = 0$.

Composite prestressed steel strand (Figure 1):

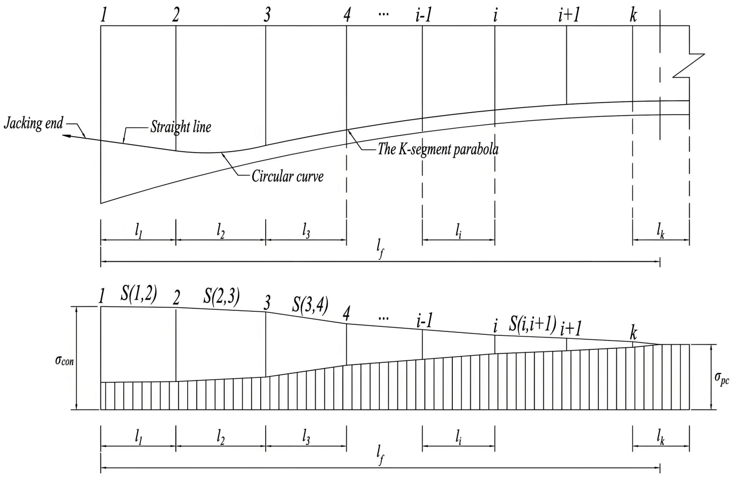

Figure 1. Schematic diagram of composite steel bundle

$$\sigma_{l1} = \sigma_{con}\left(1 - e^{-\left(\sum_{j=1}^{i-1} K'_j l_j + K'_i x\right)}\right) \tag{2}$$

In the formula: K': Comprehensive impact coefficient of the pipeline, see Table 1 for details.

Table 1. Key parameters of our model

Geometric Configuration	Comprehensive Impact Coefficient of the Pipeline K'	
Straight line	k	
Vertical circular curve	$\frac{\mu}{R_1} + k$	R_1-Radius of the vertical circular curve
Horizontal circular curve	$\frac{\mu}{R_2} + k$	R_2-Radius of the horizontal circular curve
Combined horizontal and vertical circular curve	$\frac{\mu}{R} + k$	R-Radius of the combined circular curve $R = R_1 R_2\sqrt{\frac{1}{R_1^2 + R_2^2}}$

2) The anchorage slip loss $\sigma_{l2}(x)$

Straight prestressed steel strands:

$$\sigma_{l2} = \frac{a}{l}E_s \tag{3}$$

In the formula: a: Deformation of the tensioning end anchorage and the internal shrinkage value of the prestressing tendons (mm). l: Distance from the tensioning end to the anchorage end (mm). E_s: Elastic modulus of the prestressing steel (N/mm^2).

Curved prestressed steel strands:

$$\sigma_{l2} = 2\sigma_{con} l_f \left(\frac{\mu}{r_c} + k\right)\left(1 - \frac{x}{l_f}\right) \tag{4}$$

Composite prestressed steel strands:

$$S_{(i,i+1)} = \frac{\sigma_{l1}(i+1) - \sigma_{l1}(i)}{l_i} = \frac{\sigma_{con} e^{-\sum_{j=1}^{i-1} K_j' l_j}\left(1 - e^{-K_i'}\right)}{l_i} \approx \sigma_{con} e^{-\sum_{j=1}^{i-1} K_j' l_j} K_i' \tag{5}$$

$$\sigma_{l2}(\boldsymbol{x}) = \begin{cases} 0 & (\boldsymbol{m} > \boldsymbol{r}) \\ 2\left(\sum_{j=1}^{m+1} \boldsymbol{l}_j - \boldsymbol{x}\right)\boldsymbol{S}_{(m,m+1)} + \sum_{j=m+1}^{r} 2\boldsymbol{l}_j \boldsymbol{S}_{(j,j+1)} + 2\left(\boldsymbol{l}_f - \sum_{j=1}^{r} \boldsymbol{l}_j\right)\boldsymbol{S}_{(k,k+1)} & (\boldsymbol{m} < \boldsymbol{r}) \\ 2\left(\boldsymbol{l}_f - \boldsymbol{x}\right)\boldsymbol{S}_{(r,r+1)} & (\boldsymbol{m} = \boldsymbol{r}, \boldsymbol{x} \le \boldsymbol{l}_f) \\ 0 & (\boldsymbol{m} = \boldsymbol{r}, \boldsymbol{x} > \boldsymbol{l}_f) \end{cases} \tag{6}$$

In the formula: l_f: Length of reverse friction effect (m). $S_{(i,i+1)}$: Slope of the segmented steel strand.

2.2 Solid Reinforcement Method-Cooling Method Principle

The cooling method is a numerical technique used to indirectly simulate prestress by replicating the thermal strains resulting from temperature changes. This approach applies a negative temperature field (cooling) within the finite element model, utilizing the material's thermal expansion coefficient to induce thermal shrinkage strains, thereby mimicking the effects of prestressing. By adjusting the cooling magnitude, the resulting thermal strains can be controlled to correspond with the desired prestress levels.

The prestress applied can be flexibly modulated by varying the cooling values assigned to the prestressing tendon elements. When accounting for prestress losses, these cooling values can be adjusted accordingly [23]. The calculation of cooling values is based on the principle that the linear strain induced by temperature changes equals the linear strain produced by axial force, which is expressed by the following formula:

$$\Delta T = \frac{\sigma_p}{\alpha E_p} \tag{7}$$

In the formula: ΔT: The applied cooling value. σ_p: Effective prestress considering prestress loss. α: Coefficient of linear thermal expansion of the prestressing tendons. E_p: Elastic modulus of the prestressing tendons.

2.3 RBF Neural Network Model Algorithm

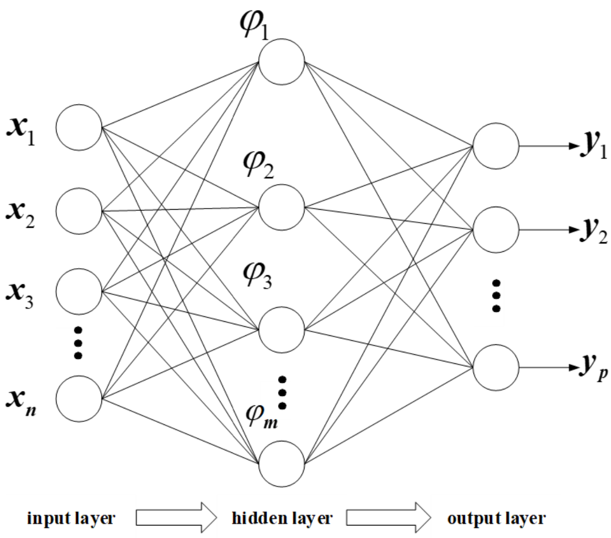

Figure 2. RBF neural network structure

Compared to other neural networks, RBF neural networks are more effective at handling complex nonlinear problems in stress prediction, especially when data is limited. Additionally, the structure of an RBF network is simple, typically containing only one hidden layer, which allows for faster convergence during training. Each node has a clear physical meaning, making the network more intuitive and easier to understand when applied to engineering problems. As a result, RBF neural networks can offer superior performance and efficiency in training surrogate models for stress prediction.

The RBF neural network is a forward neural network that solves nonlinear problems by mapping inputs into a high-dimensional space. It primarily consists of three layers: an input layer, a hidden layer, and an output layer. The core idea is to use RBF to map the input data into a high-dimensional space, enabling linearly inseparable samples to become linearly separable in this space [24].

In the network structure, the input layer directly receives the sample data from external inputs, with each node in the input layer corresponding to one dimension of the input vector. The hidden layer is the core component of the RBF neural network, using RBFs as activation functions. Each hidden node corresponds to a center (also called a centroid) and computes the distance between the input sample and the center via the RBF. The output layer performs a linear combination of the weighted sum from the hidden layer, producing the final output. As shown in Figure 2, the RBF neural network can be seen as a mapping: x $\rightarrow$ y.

Let $x = (x_1, x_2, \dots, x_n)^T, x \in R^r$ is the input vector. $y = (y_1, y_2, \dots, y_p)^T, y \in R^s$ is the output vector.

This paper primarily focuses on developing a surrogate model for predicting stress and deflection. For stress prediction, accurately capturing local features is particularly important. Compared to other commonly used RBFs, Gaussian RBFs can better reflect the variations in stress distribution within prestressed hydraulic structures. They provide superior local approximation capabilities, ensuring the model's flexibility and enhancing the overall robustness and reliability of the network. Therefore, the output of the i-th node in the hidden layer is:

$$\boldsymbol{R}_i(\boldsymbol{x}) = \exp\left[-\frac{|\boldsymbol{x} - \varphi_i|}{2\sigma_i^2}\right] \tag{8}$$

In the formula: $|\cdot|$: Euclidean norm in the input space. φ_i: The center vector of the RBF, $\varphi_i = (\varphi_{i1}, \varphi_{i2}, \dots, \varphi_{im})^T$. σ_i : The expansion width of the i-th RBF.

The output of the j-th node in the output layer is:

$$\boldsymbol{y}_j(x) = \sum_{j=1}^{m} w_{ji}\boldsymbol{R}_i(x) + w_{j0} \tag{9}$$

In the formula: w_{ji}: The connection weight from the i-th node in the hidden layer to the j-th node in the output layer. w_{j0}: The bias of the j-th node in the output layer.

R^2 is a good criterion for evaluating the fitting accuracy of surrogate models, with values typically ranging from [0,1]. The closer the value is to 1, the higher the model fitting accuracy; the closer the value is to 0, the lower the model fitting accuracy. The expression is:

$$\boldsymbol{R}^2 = 1 - \frac{\sum_{i=1}^{n} (\hat{y}_i - y_i)^2}{\sum_{i=1}^{n} (\bar{y} - y_i)^2} \tag{10}$$

Mean square error expression:

$$MSE = \frac{1}{n}\sum_{i=1}^{n} (y_i - \hat{y}_i)^2 \tag{11}$$

Mean absolute error expression:

$$\boldsymbol{MAE} = \frac{1}{n}\sum_{i=1}^{n} |\boldsymbol{y}_i - \hat{\boldsymbol{y}}_i| \tag{12}$$

In the formula: n: The number of samples. $\hat{y}_i$: The predicted value of the i-th output. y_i: The simulated value of the i-th output. $\bar{y}$: The mean of the y values among n sample points.

3 Engineering Case

3.1 Engineering Overview

The Dongjiacun aqueduct has a total length of 238.943 m and features a simply supported prestressed C50 concrete structure with three-way prestressing. It consists of eight spans, with seven spans measuring 30 m and one span measuring 28.94 m. The aqueduct is supported by seven intermediate piers and two end piers. The piers are made of C25 reinforced concrete and have heights ranging from 6.4 m to 8.4 m.

The longitudinal prestressed steel strands are arranged in two forms: arc-shaped and straight. The longitudinal arc-shaped prestressed steel strands are placed within the side walls and central wall, while the straight longitudinal prestressed steel strands are positioned at the bottoms and tops of the side walls, central wall, and bottom slab.

The steel strands in the beams feature both straight and arc-shaped peak-valley curves. The arc-shaped peak-valley prestressed steel strands are placed within the web of the beams, while the straight prestressed steel strands are located in the flanges of the beams, forming a grid pattern orthogonal to the longitudinal steel strands in the bottom slab. The vertical prestressed steel bars are arranged in a straight line and are placed within the edge ribs, central wall, and side walls.

The specific arrangement of prestressing tendons in the single-span aqueduct is as follows: All vertical prestressed steel bars use PSB930 grade $\varphi^{ps}32$ rolled threaded steel. The longitudinal prestressed steel strands at the bottom of the edge beams and part of the central beams use $7\Phi^{S}15.2$; the middle of the edge beams and part of the central beams use straight strands of $9\Phi^{S}15.2$; the bottom slab longitudinally uses $4\Phi^{S}15.2$; the bent steel strands in the central beam use $11\Phi^{S}15.2$; the pedestrian walkway slabs under the edge beams and central beams use $3\Phi^{S}15.2$; and the transverse prestressed steel strands in the bottom slab use $3\Phi^{S}15.2$, while the peak-valley shape in the bottom ribs uses $11\Phi^{S}15.2$.

The mechanical parameters of the concrete materials, steel strands, and threaded rebar are shown in Table 2.

Table 2. Mechanical parameters of materials table

Material Category	Elastic Modulus (Pa)	Poisson's Ratio	Density $(\mathrm{Kg/m^3})$	Coefficient of Linear Expansion
Concrete	3.45×10^{10}	0.2	2500	1×10^{-5}
Steel strands	1.95×10^{11}	0.3	7800	1×10^{-5}
Threaded rebar	2×10^{11}	0.3	7800	1×10^{-5}

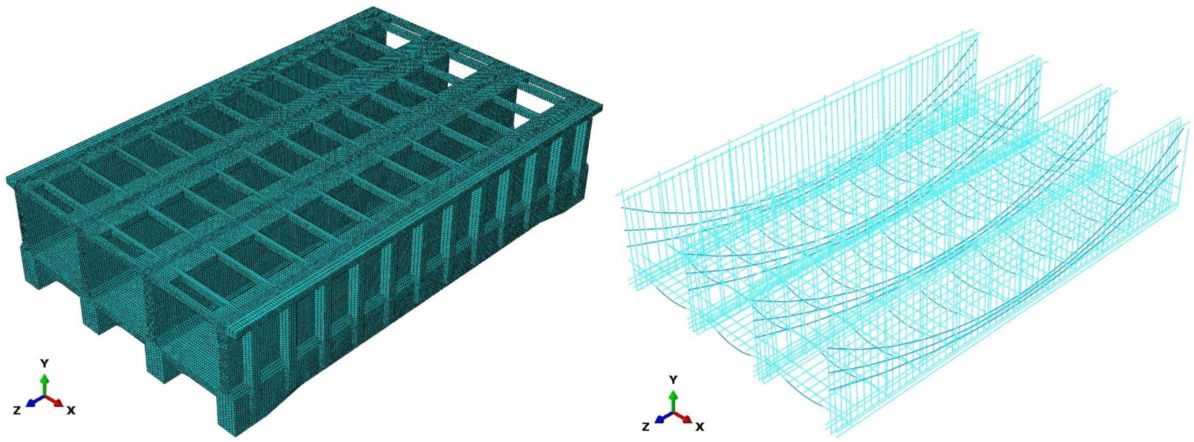

(a)

(b)

Figure 3. Finite element model (a) Aqueduct finite element model (b) Steel strand finite element model

Table 3. Cooling value

Type of Prestressed Steel Strands	Standard Value of Tensile Strength (MPa)	Tension Control Stress (MPa)	Cooling Value (°C)
Longitudinal straight steel strands	1860	1302	-611
Longitudinal curved steel strand	1860	1302	-565∼-622
Transverse straight steel strand	1860	1302	-616
Transverse valley-peak steel strand	1860	1302	-478∼-597
Vertical threaded rebar	1080	756	-280

Note: The tension control stress is 0.7 times the standard value of tensile strength

The boundary conditions for the aqueduct structure adopt a spatially simply supported constraint form, ensuring that both longitudinal and transverse constraints of the aqueduct structure are simply supported. The three-dimensional finite element model of the aqueduct body is shown in subgraph (a) of Figure 3, while the prestressed steel strand model is shown in subgraph (b) of Figure 3. The model consists of a total of 438,938 nodes and 358,984 elements, of which there are 329,928 C3D8R elements and 29,056 T3D2 elements.

The cooling application values are shown in Table 3.

3.2 Acquisition of Tension Monitoring Points

Monitoring points should be scientifically distributed based on the actual conditions of the structure to ensure a comprehensive reflection of stress changes during the loading process. First, identify the key stress locations in the structure, such as the tensioning end and the mid-span position. Then, distribute the monitoring points evenly across the overall structure to obtain global stress change information, while appropriately increasing the density of monitoring points in critical areas to enhance the ability to discern local stress variations. Finally, consider the locations of boundary conditions, as they can effectively reflect the impact of boundary effects on stress.

Using FEA to assist in point selection is a key step in analyzing the prestress transfer mechanism and the overall mechanical performance of the aqueduct. The specific process is shown in Figure 4.

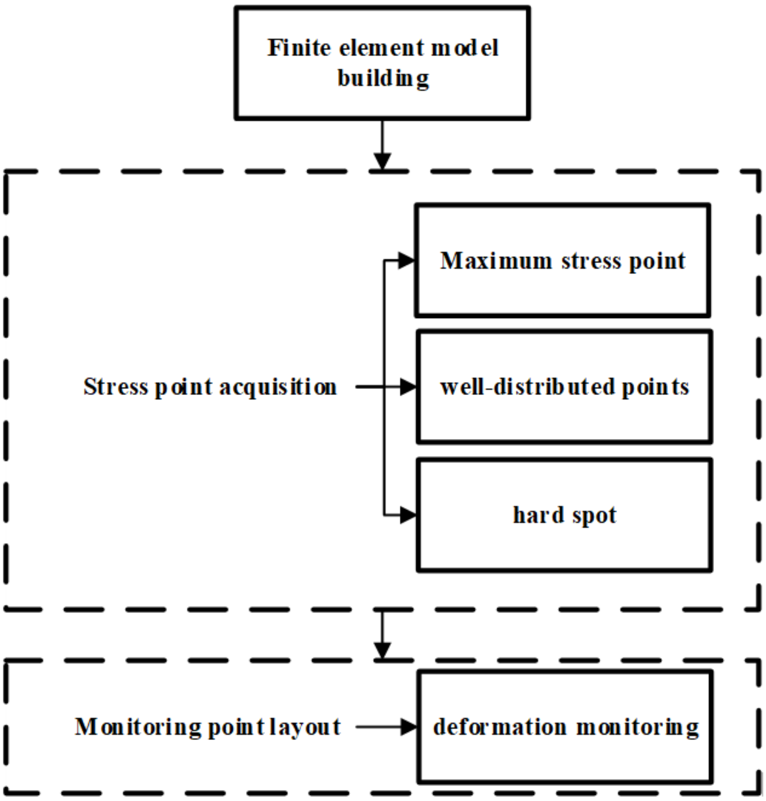

Figure 4. Flowchart for selecting monitoring points

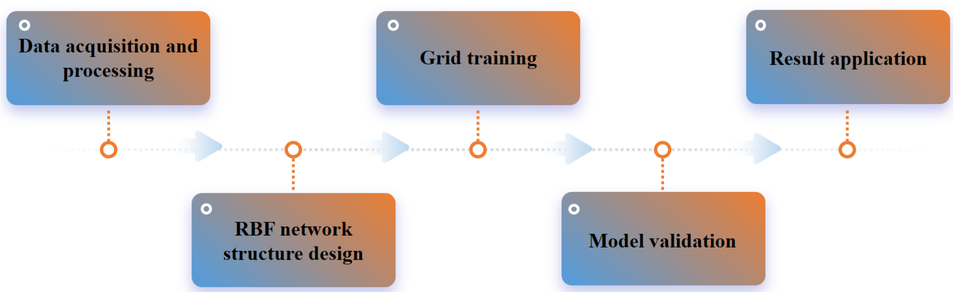

Figure 5. Flowchart of the surrogate model

Based on the aqueduct structure, a finite element model is established, considering factors such as the nonlinear material properties of the aqueduct concrete, water load effects, contact characteristics, and complex boundary conditions to accurately reflect the mechanical behavior of the aqueduct during the tensioning process. By analyzing the evolution of stress distribution, key points in various tensioning processes can be precisely identified, such as the initial stress point, maximum stress point, and stress transfer point. Additionally, by monitoring the displacement-time curve of the aqueduct structure during the tensioning process, the amount of deformation that occurs in the aqueduct during the transfer of tension forces can be identified, particularly at large spans, support points, or weak sections of the aqueduct, which are typically areas where deformation concentrates.

Surrogate model

The surrogate model training method based on RBF neural networks can effectively replace traditional finite element simulations to rapidly predict key characteristic points and mechanical behavior during the tensioning process of the aqueduct. The implementation steps are shown in Figure 5.

First, data such as stress and displacement during the tensioning process are obtained through finite element simulations, and this data is normalized and processed for outliers to serve as training samples for the RBF neural network. Next, a reasonable RBF network structure is designed, with the input layer containing parameters such as tension force and strand position. The hidden layer processes the input data by applying a Gaussian function to the distances from the center points, while the output layer is used to predict physical quantities such as stress and displacement during the tensioning process.

During the training process, the network weights are optimized using the least squares method or gradient descent, and the kernel function parameters are adjusted through cross-validation. After training is complete, the model is validated using data that was not involved in the training to ensure good generalization capability. Ultimately, this surrogate model can quickly and accurately predict the stress and displacement distribution at various monitoring points within the aqueduct structure when the input parameters are known, providing an efficient numerical tool for the optimization design and performance evaluation of the tensioning process.

Although RBF neural networks demonstrate strong nonlinear approximation capabilities and fast convergence speeds in stress and displacement prediction, there are still some potential limitations in practical applications, as follows:

1. When handling large-scale, high-dimensional data, RBF networks are prone to overfitting and a decrease in computational efficiency.
2. The expansion width of the RBF requires extensive experimentation for tuning; improper selection can lead to overfitting or underfitting, reducing the model's prediction accuracy.
3. The model lacks robustness.

To address the limitations of RBF neural networks, the following improvement directions are proposed:

1. Introduce more effective dimensionality reduction methods to optimize input data and reduce redundant features, thereby enhancing the performance of RBF neural networks with large-scale data.
2. Utilize automated hyperparameter optimization techniques to accurately adjust key parameters in the RBF network, such as the width of the basis function and the number of nodes, thereby improving the model's approximation ability and generalization performance.
3. Enhance the performance and generalization capability of the RBF network on complex datasets by constructing deep RBF networks or hybrid models that leverage the feature extraction capabilities of deep learning.

4 Design of an Intelligent Monitoring Platform for the Tensioning Process of Concrete Aqueducts

4.1 System Architecture Design

The overall architecture design of the intelligent monitoring platform for the tensioning process of concrete aqueducts includes a multi-level, modular system layout that ensures efficient collaboration among data collection, transmission, processing, analysis, and visualization. To achieve this goal, the focus is on the following aspects, as shown in Figure 6.

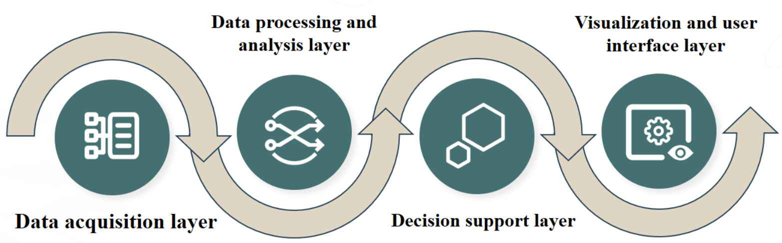

Figure 6. Overall architecture design diagram

First, the data acquisition layer monitors key parameters during the tensioning process of the aqueduct in real-time by deploying sensors for stress, strain, displacement, temperature, and other factors. The data is transmitted to the data transmission layer via wired or wireless networks, ensuring efficient and stable transmission of sensor data.

Next, the data processing and analysis layer integrates big data processing techniques and intelligent algorithms. Using neural networks and FEA models, it normalizes real-time monitoring data, conducts anomaly detection, and fuses multi-source data to generate accurate results for stress distribution, displacement changes, and prestress loss.

Then, the decision support layer incorporates an automatic early warning mechanism and intelligent prediction functions. It provides warnings and optimization suggestions based on comparisons between real-time data and thresholds, assisting users in adjusting operations during the tensioning process in real-time.

Finally, the visualization and user interface layer offer an interactive graphical interface that presents monitoring data, historical trends, and prediction results intuitively through 3D models, curves, and other means, making it convenient for users to view, analyze, and export relevant reports.

The entire system architecture supports distributed monitoring, remote access, and high scalability, ensuring safe, precise monitoring and long-term performance evaluation during the tensioning process of the aqueduct.

4.2 Prestress Monitoring and Prediction

Prestress monitoring and prediction are core functions of the intelligent monitoring platform for concrete aqueducts, encompassing real-time prestress monitoring, data analysis, and loss prediction. The aim is to ensure effective transmission of tension forces and maintain the long-term safety of the structure. The system should achieve precise performance management through sensor monitoring, intelligent analysis algorithms, and historical data processing. Specifically, it includes the following five major aspects:

1. Real-time Prestress Monitoring: The core of real-time prestress monitoring lies in the measurement of stress, strain, and prestress loss to ensure that the tension force is transmitted to the strands as designed. Sensors are deployed at critical locations such as the anchorage end, tensioning end, and mid-span to monitor the stress transfer in the strands and the concrete's stress response. Simultaneously, sensors continuously collect displacement and temperature data, and high-frequency data acquisition and processing ensure that stress changes during the tensioning process are captured in real time, with data presented in a visual format.

2. Prestress Loss Monitoring: The system evaluates losses caused by friction and anchorage slip by monitoring stress and displacement at the anchorage end and the middle section of the strands. Given the significant impact of anchorage slip and friction, real-time control is necessary.

3. Prestress Prediction Model: The RBF neural network is utilized for predicting prestress loss. The model learns from historical data to accurately predict future stress changes. FEA provides preliminary predictions of prestress distribution, which are optimized by combining with real-time monitoring data. Multi-source data fusion further enhances prediction accuracy, simulating prestress changes under different working conditions to support the best tensioning scheme.

4. Validation and Correction of Prediction Results: The system compares the predicted results with actual monitoring data for validation, correcting the model when discrepancies are significant. Through long-term data, the ML model can adaptively adjust, gradually improving prediction accuracy to ensure the predicted results align with reality.

5. Prestress Warning and Control: Based on the prediction results, the system designs a warning mechanism that triggers an alert when prestress loss exceeds safety thresholds, prompting the implementation of measures. In an automated system, the platform can automatically adjust the tension force based on real-time data and prediction results to ensure the safety of the tensioning process.

Through real-time monitoring, intelligent prediction, and warning mechanisms, the prestress monitoring system ensures the safety and precision of the tensioning process, providing technical support for the long-term safe operation of the aqueduct.

4.3 Visualization and User Interface Design

This paper is based on the mature Mock Plus software, which, in combination with target requirements and functional module division, has designed and constructed a prototype of the platform system. During the development of the prototype, special emphasis was placed on the intuitive design of the user interface and the smoothness of the operational workflow. Utilizing the real-time preview and interactive features provided by Mock Plus, user experience testing was conducted efficiently, and continuous optimization iterations were made based on the feedback from the tests. After multiple improvements, the final system design not only meets user needs but also enhances the user experience, optimizing the system's usability and accessibility.

(1) The login interface of the intelligent monitoring system for the prestress tensioning process of the Dongjiacun aqueduct is shown in Figure 7. The right side is the main functional area, providing account password registration and QR code login features, enhancing user convenience and security.

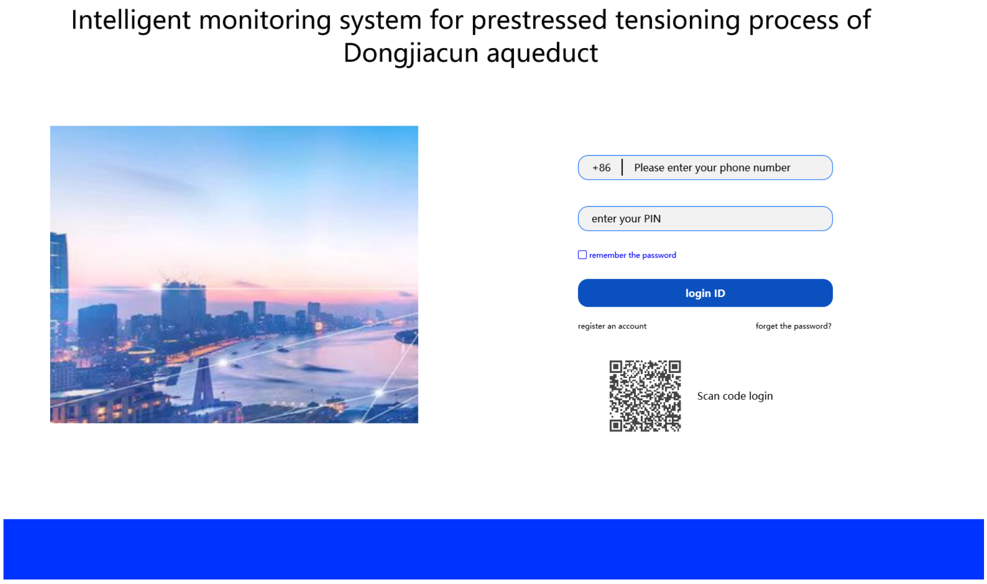

Figure 7. Design of the login interface

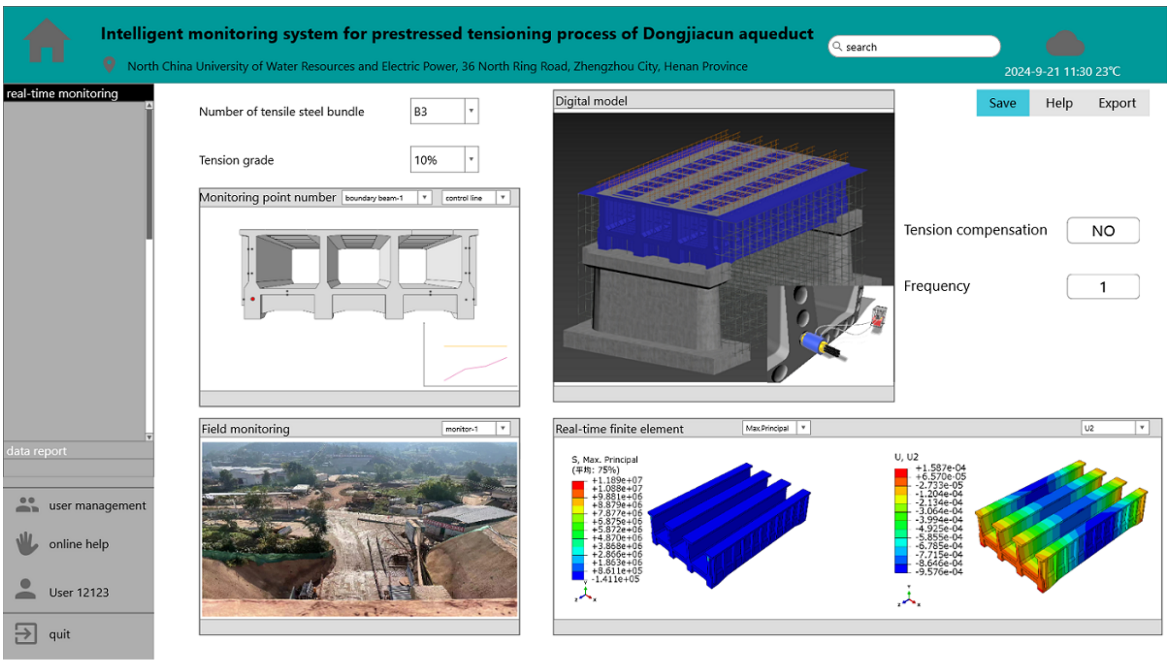

Figure 8. Operation interface

(2) The operation interface of the intelligent monitoring system for the prestressing tensioning process of the Dongjiacun aqueduct is shown in Figure 8. It integrates multiple functional modules to achieve comprehensive monitoring and management of the tensioning process. The system provides functions such as tensioning data entry, stress curve viewing, and image monitoring through the functional navigation bar on the left side. The main display area on the right shows real-time information about the tensioned steel strands, a three-dimensional stress distribution model, and images from the construction site. The stress distribution graphic, combined with FEA, visually reflects the stress conditions at various locations. Users can input the steel strand number and tensioning level in the interface and determine whether additional adjustments are necessary. The system also supports management of the number of adjustments. Through digital simulation, on-site image monitoring, and the adjustment function, the system achieves real-time monitoring and adjustment of the prestressing tensioning process, ensuring the precision and safety of the tensioning construction, making it suitable for intelligent management during the construction of large aqueduct structures.

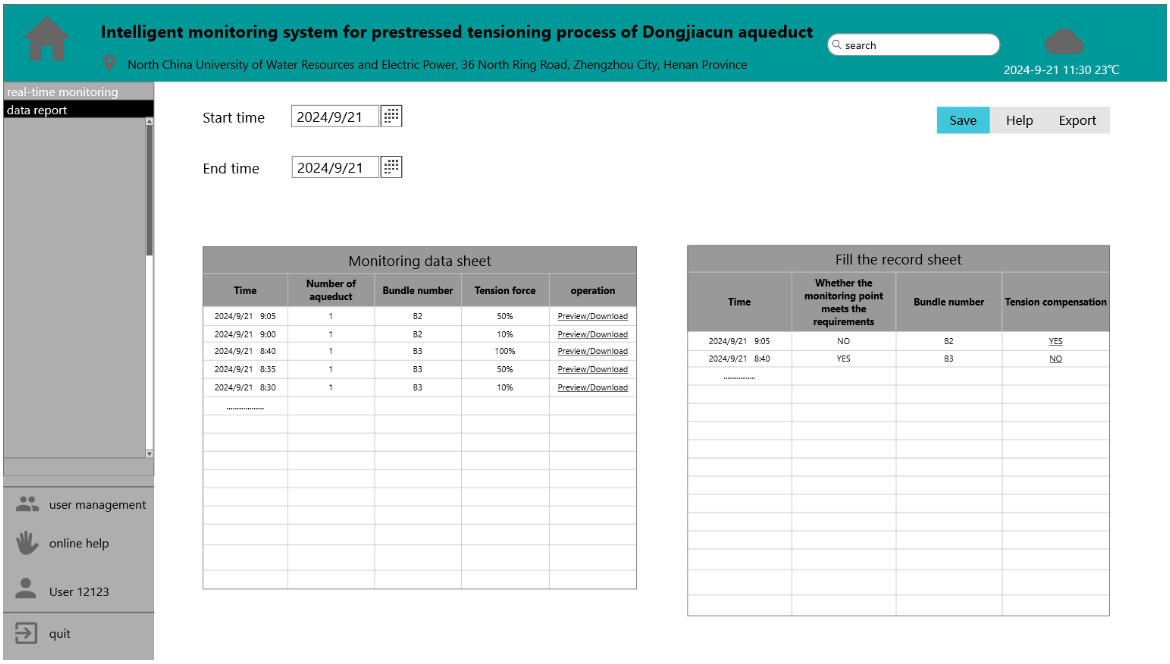

Figure 9. Design of the data recording module

(3) The data recording module of the intelligent monitoring system for the prestressing tensioning process of the Dongjiacun aqueduct is shown in Figure 9. This module provides detailed management of tensioning monitoring data and adjustment records. Its features include setting the start and end times for monitoring to filter data for specific periods. The table on the left displays the tensioning data for various measurement points on different dates, including measurement point numbers, steel strand numbers, tensioning levels, tension forces, and remarks, which help monitor real-time stress changes during the tensioning process. The table on the right specifically records adjustment operations, showing the operation date, steel strand number, number of adjustments, and whether an adjustment is needed, ensuring that the tension force of the steel strands meets design requirements. The page also provides save, delete, and export functions, facilitating user data management and subsequent analysis. Overall, the system ensures the smooth progress of the prestressing tensioning process and the long-term stability of the structure by offering comprehensive data recording and management functions.

5 Conclusion

This paper proposes an intelligent monitoring method for the prestressing process of concrete aqueducts based on RBF neural networks and FEA technology. It also designs a corresponding real-time monitoring platform to improve the accuracy and efficiency of stress monitoring during the prestressing process. In the study, a finite element model is constructed to obtain key stress data during the tensioning process, and an efficient stress prediction model is developed by integrating the RBF neural network to predict the stress distribution and prestress loss in the concrete during the tensioning process.

Compared to traditional stress monitoring methods, the intelligent monitoring platform proposed in this paper features enhanced real-time capabilities and automation. It can dynamically capture stress changes during the prestressing process and predict future stress states using big data processing and neural network technology. Additionally, the platform integrates an intelligent early warning function, which can automatically trigger an alert mechanism when abnormal stress changes are detected, ensuring the safety of the construction process. The platform also offers an intuitive visualization interface that displays real-time stress curves, three-dimensional stress distributions, and images of the construction site, significantly improving user experience and monitoring efficiency. Future research can involve surveying users to collect and analyze feedback on platform operation, providing important references for system design and functionality optimization. This will enhance the user-friendliness and usability of the platform, ensuring its effectiveness in practical applications.

The research presented in this paper demonstrates that future stress changes can be predicted using RBF neural networks in conjunction with finite element technology. Additionally, digital twin technology can generate visualized health monitoring reports to assist in decision support and predictive maintenance, effectively addressing the issues of poor real-time performance, limited monitoring points, and the challenges of accurately predicting prestress loss associated with traditional monitoring methods. The results indicate that this intelligent monitoring system can provide strong technical support for prestress control, structural health monitoring, and long-term performance evaluation of concrete aqueducts, showcasing significant engineering application value and prospects for widespread adoption. In the future, the historical stress data stored in the DT can be utilized for the continuous optimization and training of the RBF neural network model. Through the accumulation of long-term historical data, the model will be able to more accurately capture the stress change patterns of the structure, thereby improving the reliability and accuracy of predictions.

Data Availability

The data used to support the findings of this study are available from the corresponding author upon request.

Conflicts of Interest

The authors declare that they have no conflicts of interest.

References

[1] R. Alizadeh, J. K. Allen, and F. Mistree, "Managing computational complexity using surrogate models: A critical review," *Res. Eng. Des.*, vol. 31, no. 3, pp. 275–298, 2020. https://doi.org/10.1007/s00163-020-00336-7

[2] Y. Yamanaka, S. Matsubara, N. Hirayama, S. Moriguchi, and K. Terada, "Surrogate modeling for the homogenization of elastoplastic composites based on RBF interpolation," *Comput. Methods Appl. Mech. Eng.*, vol. 415, p. 116282, 2023. https://doi.org/10.1016/j.cma.2023.116282

[3] J. Kůdela and R. Matoušek, "Combining Lipschitz and RBF surrogate models for high-dimensional computationally expensive problems," *Inf. Sci.*, vol. 619, pp. 457–477, 2023. https://doi.org/10.1016/j.ins.2022.11.045

[4] F. Evangelista Junior and I. F. Almeida, "Machine learning RBF-based surrogate models for uncertainty quantification of age and time-dependent fracture mechanics," *Eng. Fract. Mech.*, vol. 258, p. 108037, 2021. https://doi.org/10.1016/j.engfracmech.2021.108037

[5] F. Antonello, J. Buongiorno, and E. Zio, "Physics informed neural networks for surrogate modeling of accidental scenarios in nuclear power plants," *Nucl. Eng. Technol.*, vol. 55, no. 9, pp. 3409–3416, 2023. https://doi.org/10.1016/j.net.2023.06.027

[6] L. Cao, S. Gong, Y. Tao, and S. Duan, "A RBFNN based active learning surrogate model for evaluating low failure probability in reliability analysis," *Probab. Eng. Mech.*, vol. 74, p. 103496, 2023. https://doi.org/10.1016/j.probengmech.2023.103496

[7] S. Gholizadeh and O. A. Samavati, "Structural optimization by wavelet transforms and neural networks," *Appl. Math. Model.*, vol. 35, no. 2, pp. 915–929, 2011. https://doi.org/10.1016/j.apm.2010.07.046

[8] F. Kazemi and R. Jankowski, "Machine learning-based prediction of seismic limit-state capacity of steel moment-resisting frames considering soil-structure interaction," *Comput. Struct.*, vol. 274, p. 106886, 2023. https://doi.org/10.1016/j.compstruc.2022.106886

[9] L. Goliatt, R. S. Mohammad, S. I. Abba, and Z. M. Yaseen, "Development of hybrid computational data-intelligence model for flowing bottom-hole pressure of oil wells: New strategy for oil reservoir management and monitoring," *Fuel*, vol. 350, p. 128623, 2023. https://doi.org/10.1016/j.fuel.2023.128623

[10] A. Abdedou and A. Soulaïmani, "A non-intrusive reduced-order modeling for uncertainty propagation of time-dependent problems using a b-splines bézier elements-based method and proper orthogonal decomposition: Application to dam-break flows," *Comput. Math. Appl.*, vol. 102, pp. 187–205, 2021. https://doi.org/10.1016/j.camwa.2021.10.006

[11] V. Mokarram and M. R. Banan, "An improved multi-objective optimization approach for performance-based design of structures using nonlinear time-history analyses," *Appl. Soft Comput.*, vol. 73, pp. 647–665, 2018. https://doi.org/10.1016/j.asoc.2018.08.048

[12] S. Bagheri, U. Reinicke, D. Anders, and W. Konen, "Surrogate-assisted optimization for augmentation of finite element techniques," *J. Comput. Sci.*, vol. 54, p. 101427, 2021. https://doi.org/10.1016/j.jocs.2021.101427

[13] V. Gribniak, G. Kaklauskas, S. Idnurm, and D. Bačinskas, "Finite element mesh size effect on deformation predictions of reinforced concrete bridge girder," *Balt. J. Road Bridge Eng.*, vol. 5, no. 1, pp. 19–27, 2010. https://doi.org/10.3846/bjrbe.2010.03

[14] N. M. Nguyen, W. C. Wang, and M. T. Cao, "Early estimation of the long-term deflection of reinforced concrete beams using surrogate models," *Constr. Build. Mater.*, vol. 370, p. 130670, 2023. https://doi.org/10.1016/j.conbuildmat.2023.130670

[15] S. Panda, A. Banerjee, and B. Manna, "Surrogate based prediction models for elastically supported beams under the action of opposite moving loads," *Structures*, vol. 54, pp. 1452–1464, 2023. https://doi.org/10.1016/j.istruc.2023.05.117

[16] H. Nguyen, T. Vu, T. P. Vo, and H. T. Thai, “Efficient machine learning models for prediction of concrete strengths,” *Constr. Build. Mater.*, vol. 266, p. 120950, 2021. https://doi.org/10.1016/j.conbuildmat.2020.120950

[17] S. Dou, J. Li, and F. Kang, “Health diagnosis of concrete dams using hybrid FWA with RBF-based surrogate model,” *Water Sci. Eng.*, vol. 12, no. 3, pp. 188–195, 2019. https://doi.org/10.1016/j.wse.2019.09.002

[18] P. G. Asteris, A. D. Skentou, A. Bardhan, P. Samui, and K. Pilakoutas, “Predicting concrete compressive strength using hybrid ensembling of surrogate machine learning models,” *Cem. Concr. Res.*, vol. 145, p. 106449, 2021. https://doi.org/10.1016/j.cemconres.2021.106449

[19] L. Wang, H. Liu, F. Zhang, L. Guo, and Z. Chen, “Spatial structure digital twins: application in intelligent health monitoring of cable dome structures,” *Autom. Constr.*, vol. 165, p. 105489, 2024. https://doi.org/10.1016/j.autcon.2024.105489

[20] S. C. Jayasinghe, M. Mahmoodian, A. Sidiq, T. M. Nanayakkara, A. Alavi, S. Mazaheri, F. Shahrivar, F. Sun, and S. Setunge, “Innovative digital twin with artificial neural networks for real-time monitoring of structural response: A port structure case study,” *Ocean Eng.*, vol. 312, p. 119187, 2024. https://doi.org/10.1016/j.oceaneng.2024.119187

[21] Ministry of Water Resources of the People’s Republic of China, “Design specification for hydraulic concrete structures: SL 191-2008,” China Water Resources and Hydropower Press, Beijing, Tech. Rep., 2008.

[22] S. He, “Research on prestress detection technology for large and medium span concrete bridges,” Ph.D. dissertation, Chang’an University, Shaanxi Province, 2009.

[23] L. He and J. Wang, “Equivalent load-real force reinforcement cooling method for simulating effective prestress,” *Highw. Traffic Technol.*, vol. 32, no. 11, pp. 75–80, 2015.

[24] X. Wang and H. Shao, “The theory of RBF neural networks and its applications in control,” *Inf. Control*, vol. 26, no. 4, pp. 272–284, 1997.